RESEARCH ARTICLE

ADVANCED OPTICAL MATERIALS
www.advopticalmat.de

Suppressed Stokes Shifts and Hot Luminescence from Quantum Dots within Plasmonic Nanocavities

*Junyang Huang, Shu Hu, Adam Roach, Angus Crookes, Niclas S. Mueller, Junzhi Ye, Lukas A. Jakob, Yuling Xiong, Shijie Zhu, Akshay Rao, Angela Demetriadou, Liangfeng Sun, and Jeremy J. Baumberg**

Lead sulfide (PbS) quantum dots (QDs) hold great promise for solar energy conversion, yet their efficiency is compromised by a substantial Stokes shift that adversely affects their performance in photonic devices. Here, PbS QDs are integrated within single plasmonic nanocavities, significantly mitigating Stokes shifts through Purcell enhancement of their band edge emission. This approach entails bottom-up assembly of QDs into nanoparticle-on-mirror structures, leading to direct emission from band-edge excitons with radiative lifetimes suppressed below 1 ns, a drastic decrease from the 1600 ns observed in unmodified QDs. This manipulation of the Stokes shift is attributed to the increased photonic density of states within the nanocavity, which accelerates the radiative decay process and modifies exciton relaxation pathways. These results underscore the critical role of plasmonic nanocavities in modifying QD emission characteristics, offering opportunities for enhancing QD-based device performance across a spectrum of photonic applications.

1. Introduction

Colloidal quantum dots (CQDs) based on lead sulfide (PbS) have emerged as a promising material in photovoltaics thanks to their outstanding solar conversion performance.[1–3] However, one of the key challenges to their application is the particularly large Stokes shift (hundreds of meV) where the emission spectrum is redshifted from the absorption spectrum.[4,5] This property, critical to the efficiency and application of semiconductor CQDs, plays a dual role depending on the application context. For QD-based light-emitting diodes, a minimal Stokes shift gives a well-populated bright band edge state with a short radiative lifetime, enabling high quantum yields through efficient competition with non-radiative processes.[6] In photovoltaic applications, Stokes shifts restrict device efficiency by reducing the open-circuit voltage due to the mismatch between optical and electronic bandgaps. Conversely, applications such as solar concentrators[7–10] and lasers[11–13] benefit from a larger Stokes shift, to minimize reabsorption of emission and enhance performance. Mastering control over this Stokes shift is thus crucial for optimizing the performance of CQD-based devices across a spectrum of applications.

The origin of the Stokes shift across different QD systems has been widely explored. The Stokes shift in CdSe QDs is ascribed to an excitonic fine structure near the band edge, associated with spin-forbidden dark excitons.[14,15] These dark excitons, undetectable in absorption, play a dominant role in photoluminescence (PL) as they form a lower energy reservoir with an extended lifetime.[16–18] This energy splitting between dark and bright excitons leads to the Stokes shift. However, the energy difference between bright and dark excitons in lead chalcogenide QD systems is relatively small (≈20 meV), insufficient to account for the observed redshifts exceeding 200 meV.[4,5,19–22] These observed redshifts at room temperature have so far been attributed to kinetic access of defect states located within the bandgap,[23] where specific intrinsic defects can cause electron density localization of the band edge states, leading to pronounced Franck–Condon shifts on the order of hundreds of meV.[24]

Coupling QDs to optical cavities can modify their Stokes shift and enhance photonic properties.[25] In general, QD emission

J. Huang, S. Hu[+], N. S. Mueller[++], J. Ye, L. A. Jakob, Y. Xiong, S. Zhu, A. Rao, J. J. Baumberg
Cavendish Laboratory
Department of Physics
University of Cambridge
JJ Thompson Avenue, CA CB3 0HE, UK
E-mail: jjb12@cam.ac.uk

A. Roach, L. Sun
The Center for Photochemical Sciences
Department of Physics and Astronomy
Bowling Green State University
Bowling Green, OH 43403, USA

A. Crookes, A. Demetriadou
School of Physics and Astronomy
University of Birmingham
Edgbaston, Birmingham B15 2TT, UK

The ORCID identification number(s) for the author(s) of this article can be found under https://doi.org/10.1002/adom.202500275

[+]Present address: Department of Physics, Xiamen University, Xiamen 361005, China

[++]Present address: Department of Physical Chemistry, Faradayweg 4-6, 14195 Berlin, Germany

DOI: 10.1002/adom.202500275

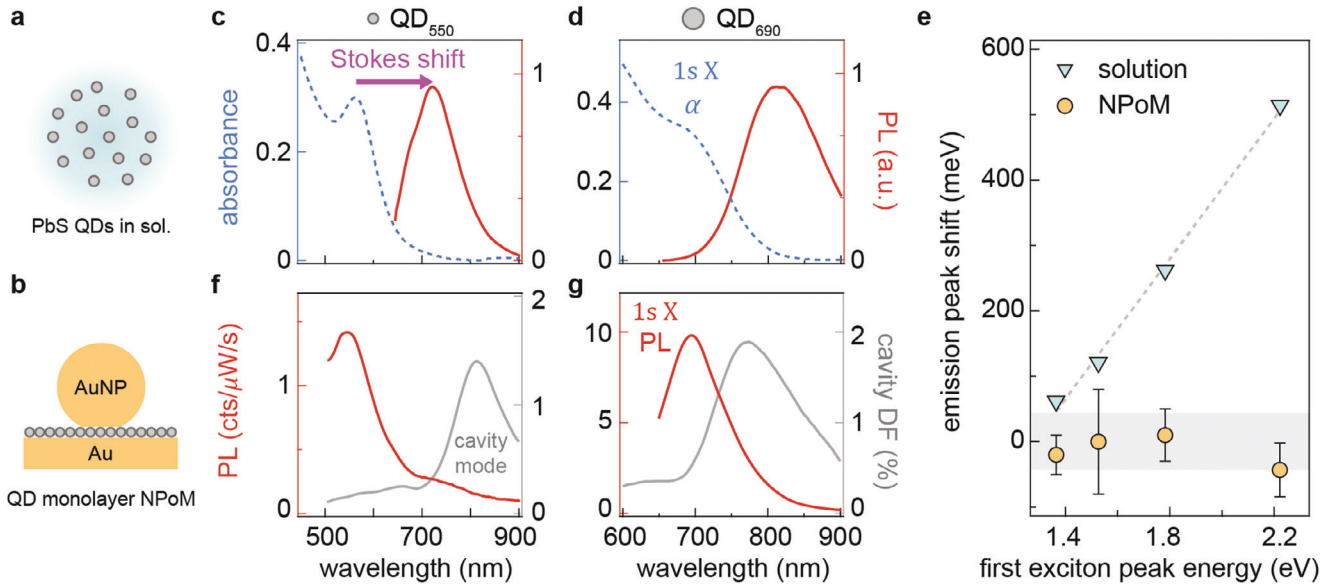

Figure 1. NPoM-modified PbS QD emission. a,b) Schematics of (a) bare PbS QDs in solution and (b) a QD monolayer integrated within single NPoM nanocavities. c,d) Absorption (α) spectra of PbS QDs with two different sizes (QD_{550} in c, QD_{690} in d) in solution (blue-dashed lines), along with their PL spectra (red solid lines) showing Stokes shifts. e) Redshift of emission peak position relative to the first exciton absorption peak for QD solution (cyan) and QD NPoM (yellow). f,g) PL spectra (red) obtained from (f) QD_{550} and (g) QD_{690} embedded in NPoMs, using 447 and 633 nm CW excitation and the corresponding dark-field (DF) scattering resonances (gray). A 500 nm long-pass filter and 633 nm notch filter are used to reject laser light in detection. Each spectrum is averaged over >80 individual NPoMs.

can be manipulated across a wide energy spectrum by amplifying specific vibronic/excitonic transitions via resonance enhancement with coupled plasmonic structures. The pronounced near-field enhancement from resonant plasmons within nanocavities ($|E/E_0| > 100$) facilitates significant Purcell enhancement of their spontaneous emission rates for both solid-state and molecular emitters.[26–32] Such extreme enhancement, in combination with a small optical mode volume ($V < 100$ nm^3), can be utilized to promote polaritonic optical phenomena[33,34] and also modify charge relaxation pathways,[35–38] setting the stage for minimizing the Stokes shift via hot luminescence, where radiative decay occurs from higher energy vibronic states rather than from the lowest excited state. Achieving hot luminescence hinges on creating conditions where the radiative decay from higher energy band edge states competes with the speed of internal relaxation (breaking Kasha's rule, which states that emission occurs from the lowest excited state). While molecular systems have yielded hot electroluminescence within nanotip-enhanced plasmonic nanocavities at cryogenic temperature, such effects have not been demonstrated at room temperature, nor have similar effects in QDs been demonstrated to our knowledge.[36]

Here, we integrate PbS QDs into single plasmonic nanocavities, achieving a large Purcell enhancement of their spontaneous emission rate by more than 1600-fold while eliminating the Stokes shift in PbS QD emission. This offers a route to manipulate exciton relaxation and alter the dominant radiative state of the QDs. For bare QDs, the Stokes-shifted emission lifetime is $\tau_{\text{bare QD}} = 1600$ ns, whereas integrating the QDs into a plasmonic cavity reduces their lifetime to <1 ns and elicits emission directly from the band edge exciton. The elimination of the Stokes shift is directly linked to the gap size of the plasmonic nanocavity, illustrating the critical influence of nanocavity geometry on the emission characteristics. This effect is attributed to the enhanced photonic density of states within the cavity, which significantly accelerates the radiative decay process from the band-edge state, effectively outpacing internal phonon-coupling relaxation mechanisms and thereby altering the exciton relaxation pathways. Our findings highlight the profound impact of nanophotonic engineering on the emission properties of QDs, providing a pathway for optimizing the performance of QD-based photonic devices.

2. Results and Discussion

We adopt a bottom-up approach for robustly and deterministically integrating QDs into Nanoparticle-on-Mirror (NPoM) nanocavities (Experimental Section). Briefly, a suspension of PbS QDs[39] in hexane is deposited onto a diethylene glycol (DEG) surface. Hexane evaporation leads to the formation of a close-packed monolayer of QDs at the DEG-air interface. This QD film is then transferred to a template-stripped Au surface. Subsequently, colloidal Au NPs ($D = 80$ nm) are drop-cast onto the QD monolayer to form the NPoM construct.[30] The average core diameter of the PbS QD_{690} is determined to be 1.6 ± 0.3 nm using transmission electron microscopy (TEM, Figure S1, Supporting Information). The thickness of the QD monolayer on the Au substrate, which includes oleic acid capping ligands, is measured to be 5 ± 1 nm using atomic force microscopy (AFM, Figure S2, Supporting Information). This thickness will be reduced in the NPoM nanogap due to van der Waals compression from the upper NP. Individual NPoMs are analyzed optically in a custom-built confocal microscope, using fully automated PL and dark-field scattering spectroscopy.

The extinction and emission spectra of bare PbS QDs of two distinct sizes in hexane suspension (**Figure** 1c,d) clearly show

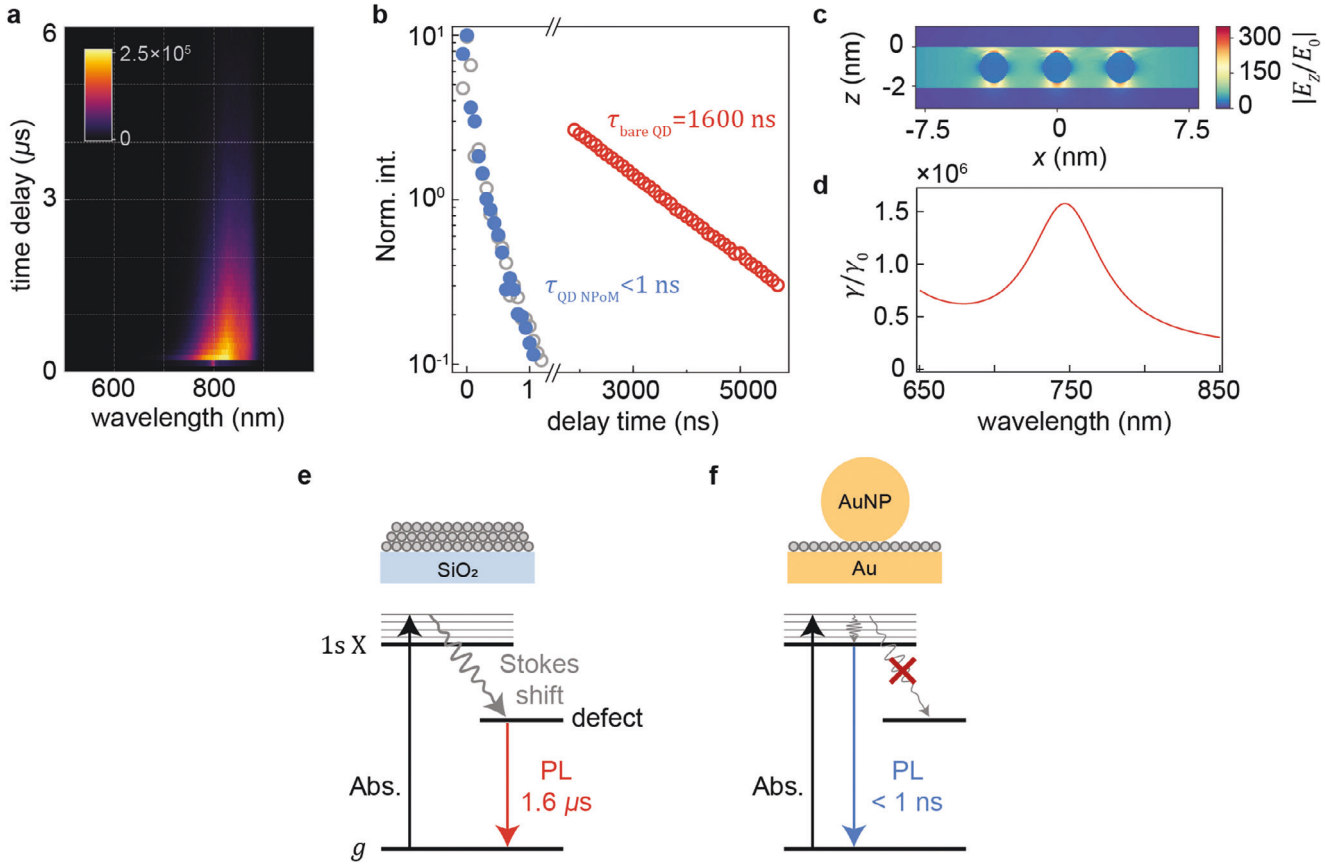

Figure 2. Purcell-accelerated emission lifetime. a) Time-gated PL trace of PbS QD_{690} multilayer on glass, with λ_l= 400 nm pulses. b) Normalized intensity versus time delay from time-gated PL from QD multilayer (red open circles), TCSPC of emission from QD NPoM (blue-filled circles), and TCSPC instrument response from Si Raman signal (gray open circles). Laser fluence of 1.2 and 0.07 μJ cm^{-2}/pulse were used, respectively. c) Simulation of the normalized electric field in the x-z plane of the QD NPoM nanocavity at an excitation wavelength of 745 nm. d) Spontaneous emission rate enhancement as a function of wavelength calculated at the top of the central QD. e) Bare QDs on glass: photoexcitation of charges followed by relaxation into defect states results in slow redshifted emission (>1 μs). f) Proposed mechanism for QDs in NPoMs: Purcell-enhanced emission from the band-edge exciton surpasses the relaxation pathway to defect states, leading to ultrafast band-edge exciton emission with suppressed Stokes shift.

the Stokes shift. The first exciton absorption peaks appear at 550 and 690 nm, respectively (dashed blue lines). Upon above-band optical excitation of these QD suspensions, PL emanating from defect states is observed at 720 and 820 nm (red lines), respectively.[23,24] The Stokes redshift between absorption and emission energy is found to be directly proportional to the first exciton peak energy (Figure 1e), concurring with previous reports.[23] In stark contrast, the emission spectra from PbS QDs within NPoM nanocavities do not exhibit a Stokes shift, resulting in emission bands that align spectrally with their first exciton absorption peaks (Figure 1f,g, red). This phenomenon implies that the NPoM nanocavity significantly modifies the exciton relaxation pathway, leading to emission directly from the band-edge exciton. This suppression of Stokes shift is consistently observed across four different QD sizes (Figure 1e). Notably, for monolayer PbS QDs outside the NPoM nanocavities, the emission is completely quenched by the Au mirror. Consequently, the PL spectra collected here, using a 1.5 μm collection spot diameter are exclusively from the cavity-enhanced emitters.

Statistics of cavity dark-field scattering resonances are collected from >100 NPoM nanocavities, yielding an average peak resonance at 810 and 770 nm (Figure 1f,g gray lines, Figure S3, Supporting Information). The blueshifted cavity resonance in the QD_{690} NPoM, compared to QD_{550}, is attributed to the increased gap size dictated by the QD diameter.[40,41] It is important to note that the observed emission bands in NPoMs do not coincide spectrally with the predominant cavity modes in the dark field spectra. Therefore, this characteristic differentiates our findings from previous studies involving nanocube-on-mirror structures with large PbS QD gap sizes, where emission was predominantly influenced by the fundamental modes of the plasmonic cavities.[26]

Time-gated PL analysis is employed to quantify the emission lifetime of the PbS QD_{690}. This measurement shows that the "bare QD" (not coupled to any photonic structure) has a lifetime $\tau_{\text{bare QD}}$ = 1600 ns within a solid film matrix (**Figure 2**a,b). Initially, the excitons are excited in high-energy band edge states, before they undergo nonradiative Stokes transitions, transferring to lower-energy defect states. Emissions from such defect states typically have extended lifetimes on μs timescales (Figure 2e), due to small electron-hole pair overlap.[23,42–44] We note that a monolayer of PbS on a glass substrate yields PL signals that are too

weak to be detected, impeding direct experimental measurement of the NPoM cavity enhancement factor.

By contrast, integrating these QDs into NPoM structures gives a significant reduction in lifetime. Emission centered ≈690 nm displays a decay on sub-nanosecond timescales (<1 ns, Figure 2b, blue). However, this rapid decay rate matches the instrumental response function of our time-correlated single photon counting (TCSPC) setup, which has a temporal resolution of 1 ns, indicating that the actual emission lifetime may be much shorter than 1 ns. (Figure 2b, gray).[45] Finite element simulations reveal that QDs positioned within the NPoM nanocavity experience substantial field enhancement ($|E/E_0| \approx 340$ at the top and bottom of QDs (Figure 2c; Figure S4, Supporting Information).

In NPoM structures, although the QD emission wavelength is offset from the fundamental cavity mode, which is the most efficient in coupling into the far field, the nanocavity supports a set of higher-order quasi-normal modes whose energy spans from the single nanoparticle plasmon resonance at ≈ 550 nm to the dominant cavity mode at 770 nm. These higher-order modes, while less pronounced in the scattering spectrum, produce substantial field enhancement within the nanogap, facilitating enhanced spontaneous emission at a broader off-resonance spectral range.

Our finite-element simulations presented in Figure 2d account for the cumulative contributions of these higher-order quasi-normal modes, demonstrating that the spontaneous emission rate enhancement remains significant at the QD emission wavelength of 690 nm, While the calculated Purcell factor can reach 10^6 under idealized conditions at the point of maximum field enhancement, we acknowledge that the enhancement experienced by a QD dipole distributed throughout its volume is expected to be more moderate in a realistic scenario. Even a more conservative enhancement on the order of 10^3 would still be sufficient to accelerate radiative recombination and suppress the Stokes shift. Although we cannot directly measure such a high Purcell factor, both the predicted and measured shortening of emission lifetime readily implies that within NPoM nanocavities the Purcell enhanced emission rate of the band edge excitons can surpass their coupling with surface defect states, which typically occurs on time scales of hundreds of picoseconds,[46,47] effectively suppressing the Stokes shift process (Figure 2f).

We compare the QD NPoM emission for a range of excitation wavelengths λ_l. The PL spectra are recorded while varying the excitation wavelength from 530 to 633 nm (**Figure 3**). Across all excitation wavelengths, the band-edge emission at 690 nm is consistently observed, and the Stokes-shifted defect emission band at 820 nm, prominent in bare PbS QDs, is absent, indicating that the suppression of the Stokes shift persists. In the spectrum with 633 nm excitation, narrower surface-enhanced Raman scattering (SERS) lines from the QD ligands are also observed (FWHM ≈ 5 nm). These inelastic SERS features shift according to the excitation wavelength, while the broader QD excitonic emission (FWHM ≈ 20 nm) remains consistently observed ≈690 nm across all excitation wavelengths.

For excitation at wavelengths ≤600 nm, an additional lower-energy emission band is detected ≈760 nm. This emission band coincides with the dark-field scattering resonance of the nanocavity (Figure 3, red-dashed curve). We note that empty NPoM cavities do not yield any photoluminescence signature (Figure S5a–c, Supporting Information). The origin of this distinct PL signature in PbS NPoM is attributed to the emission enhanced by the metal nanocavity, where the photo-induced dipole in the QDs couples to the cavity by exciting a plasmon. The subsequent radiative decay of this plasmon outcouples into free space through the dominant (10) optical nanocavity modes.[26,48–50] Our analysis reveals that the photoluminescence ratio between plasmon and exciton emissions exhibits a pronounced dependence on the laser excitation wavelength, correlating with the (20) cavity mode resonance (Figure S5d, Supporting Information).[41] This finding shows that aligning the excitation wavelength to the (20) cavity mode matches the spatial excitation profile of the QDs to the (10) cavity mode, dictates the outcoupling efficiency, and therefore leads to enhanced outcoupling at 760 nm.

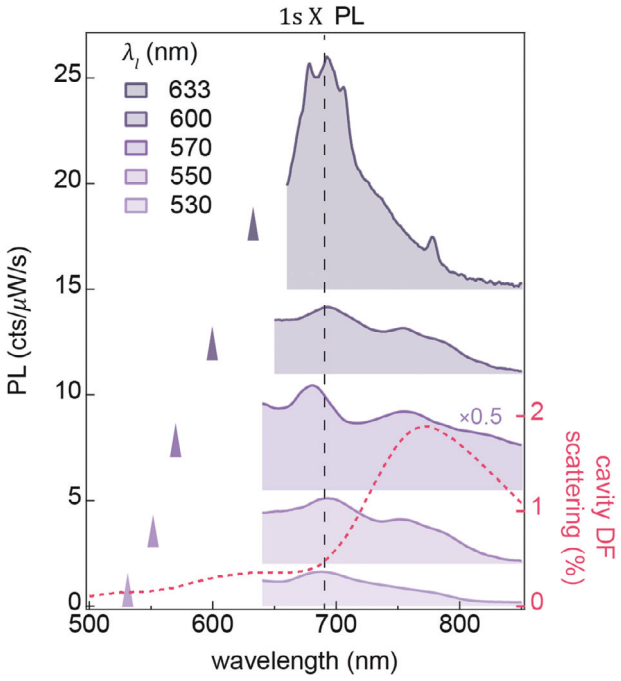

Figure 3. Excitation wavelength dependence. Normalized PL spectra from QD_{690} NPoMs while tuning excitation wavelength λ_l from 530 nm (bottom) to 633 nm (top). Optical excitation is performed with 500 fs pulses of average power <3 μW, except 633 nm with 10 μW CW laser (top). The PL spectra are taken with long path filters >630 nm, and the background of the spectra is attributed to electronic inelastic light scattering. Average dark-field scattering spectrum of NPoM nanocavities shown by red dashed curve.

The suppression of the Stokes shift is caused by the Purcell effect, which enhances the spontaneous emission rate of the band edge exciton. This phenomenon is intricately linked to the plasmonic gap size. Specifically, a larger gap reduces the field enhancement within the nanocavity, exponentially lengthening the Purcell-enhanced radiative recombination of the band-edge exciton.[27] The relationship between the field enhancement in the NPoM nanocavity (E/E_0) and its gap size (d) is given by $\frac{E^2_{max}}{E^2_0} \propto Q n_g \frac{R^2}{d^2}$, where Q is the quality factor of the resonance, n_g the refractive index of the gap, and R the radius of the nanoparticle.[31] If the Purcell effect is insufficient to counteract relaxation into

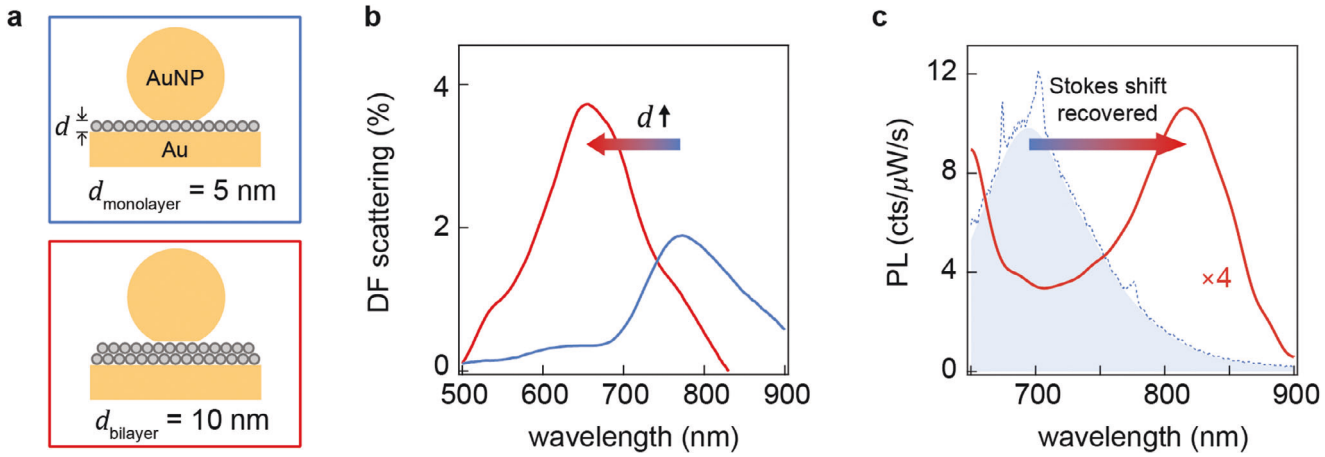

Figure 4. Gap size-dependent emission. a) Schematics of NPoM gaps defined by monolayer (blue) and bilayer (red) of QD. b) Dark-field scattering spectra of monolayer (blue) and bilayer (red) QD_{690} NPoM, with blue-shifted cavity resonance from increased gap size. c) Normalized PL spectra of monolayer (blue, removing additional ligand SERS peaks in dashed line to give PL) and bilayer (red) QD_{690} NPoM, for 633 nm CW excitation. Spectral background <670 nm is due to laser leakage.

the Stokes-shifted transition, it is anticipated that Stokes-shifted emission will re-emerge.

To validate this hypothesis, we experimentally expand the NPoM gap by incorporating a bilayer of PbS QDs within the nanocavity ($d_{bilayer}$ = 10 nm, **Figure 4a**). As anticipated, increasing the gap size blueshifts the dark-field resonance relative to the monolayer nanocavity (Figure 4b).[40,41] This blue shift arises because the weaker field confinement within the nanogap leads to a lower effective refractive index for the plasmonic mode, reducing its resonant wavelength.[31] With CW above-bandgap excitation at 633 nm, we now observe the re-emergence of Stokes shifted PL ≈810 nm in the bilayer QD NPoMs (Figure 4c). Despite the presence of a doubled density of QDs in these bilayer NPoMs, the Stokes-shifted emission is observed to be ≈ 4 times weaker compared to the band-edge exciton emission in the monolayer sample (blue line). This disparity is attributed to the reduced Purcell enhancement in the bilayer structure. We also note that using NPoM structures with a QD monolayer of a larger thickness (14 nm) formed by scaffolding with CdSe QDs also preserves the Stokes shifted emission (Figure S6, Supporting Information), as predicted in this model.

These findings address the critical challenge of the substantial Stokes shift in PbS QDs, which has limited their efficiency in photonic devices. By demonstrating significant suppression of the Stokes shift through plasmonic nanocavities, our work provides a new approach to manipulate the exciton relaxation pathway. Such Purcell accelerated emission can lead to better coherence and increased indistinguishability of photons, making it beneficial for applications in quantum information processing.

3. Conclusions

In conclusion, our study addresses the critical challenge of the substantial Stokes shift in PbS QDs, which has hindered their efficiency in photonic devices. By integrating PbS QDs with plasmonic nanocavities, we significantly manipulate the relaxation pathways, achieving over 1600-fold Purcell enhancement and complete suppression of the Stokes shift. This suppression minimizes non-radiative recombination and enhances quantum yield, making it particularly beneficial for QD-based LEDs, lasers, and other photonic applications where high brightness and fast radiative decay are advantageous. Our findings demonstrate the power of plasmonic engineering in tailoring QD emissive properties and highlight the importance of nanocavity geometry in emission control. This research lays the foundation for enhancing the performance of QD-based optoelectronic devices, while the Purcell accelerated emission also promises reduced dephasing and higher distinguishability for quantum photonic applications.

4. Experimental Section

PbS Ultrasmall QD Synthesis: Lead oxide (220 mg, 1 mmol), oleic acid (0.64 mL, 2 mmol), and 1-octadecene (9.96 mL) were refluxed and stirred under a sealed nitrogen atmosphere at 150 °C for 1 h. Then, the solution was cooled down to 50 °C and 1 mL of 1,1,2-trichloroethane was added and mixed for 30 min. In a separate flask, the sulfur precursor was prepared by adding hexamethyldisilathiane (126 µL, 0.7 mmol) dissolved in 6 mL of 1-octadecene. The solution was stirred under nitrogen protection. A 5 mL of sulfur precursor was drawn by a syringe and injected into the lead precursor. They were stirred for 2 min and then ice bathed. The product was centrifuged after mixing with toluene and acetone. The precipitated quantum dots were redispersed in toluene and stored in a dark environment.[39]

QD NPoM Assembly: To assemble QD monolayers, a colloidal PbS QD solution was first diluted to a concentration of ≈0.1 mg mL^{-1} using hexane. Then, 100 µL of this solution was spread over the surface of diethylene glycol (DEG) in a clean petri dish. By covering the petri dish, the hexane evaporates slowly over a period of 5–10 min, leading to the formation of a dense monolayer film at the DEG-air interface.[51] For the transfer of the QD film, a template-stripped Au substrate was gently brought into contact with it. As the substrate was lifted, QD monolayers of centimeter-scale were dip-coated and subsequently cleaned with 99% ethanol and dried using nitrogen gas. The thickness of the QD monolayer was characterized to be 5 ± 1 nm using atomic force microscopy, as shown in Figure S2 (Supporting Information). To create the NPoM cavity, AuNPs (BBI solutions, D = 80 nm) were sparsely drop-cast on the QD monolayer and washed with deionized water.

Optical Measurement: Dark-field microscopy and spectroscopy were performed using a customized Olympus BX51 microscope. Dark-field scattering was captured through a confocal fiber-coupled spectrometer (QE65000, Ocean Optics) that has a 1.5 µm collection spot diameter on the sample. The optical excitation of NPoMs was achieved by focusing a continuous wave laser at 447 nm (Coherent CUBE) or 633 nm (Integrated Optics) into a diffraction-limited spot through a ×100 Olympus objective (0.8 NA). PL signals were collected using the same objective, then coupled through a Triax 320 spectrometer, and finally recorded on an Andor Newton EMCCD. For wavelength-tunable excitation, a Spectra-Physics Maitai laser operating at 80 MHz was employed to drive an optical parametric oscillator (Spectra-Physics Inspire), generating 100 fs pulses. These pulses were subsequently filtered by a tunable bandpass filter (PhotonETC LLTF contrast) to 1 nm spectral width, extending the pulse duration to ≈500 fs.

Time-Gated PL Spectroscopy: The gated time-resolved PL was measured with an iCCD camera system (Andor iStarDH740 CCI-010) which was connected to a grating spectrometer (Andor SR303i). A 400 nm laser excitation was obtained from a homebuilt setup with second harmonic generation (SHG) in a BBO crystal from the fundamental output (pulse fundamental laser wavelength 800 nm, pulse length 80 fs) of a Ti:Sapphire laser system (Spectra Physics Solstice). A 425 nm long-pass filter was added in the PL collection pass to remove the residual 400 nm excitation laser. The temporal resolution of the PL emission was obtained by measuring the PL from the sample and stepping the iCCD gate delay for different delays with respect to the excitation. Measurement laser fluence was 0.064 µJ cm^{-2}/pulse.

Purcell Factor Calculations: The enhancement of the spontaneous decay rate, $P(\omega)$, was obtained by normalizing the total energy dissipation within the nanocavity

$$P_{cav} = \frac{\omega}{2} \mathrm{Im}\left(\mathrm{p}^* \cdot \mathrm{E}\left(\mathrm{r}_0\right)\right) \quad (1)$$

to the free space dissipation rate $P_0 = |\mathrm{p}|^2\, \omega^4 / 12\pi\epsilon_0 c^3$ where p is the dipole moment of a dipole with emission frequency ω at position r_0. To obtain P_{cav}, frequency domain simulations using COMSOL Multiphysics were performed, and the partial local density of states $\rho_{\mathrm{PLDOS}}(\omega) \propto \mathrm{p} \cdot Im(G(r_0, r_0, \omega)) \cdot \mathrm{p}$ as a function of frequency, where $G(r_0,r_0,\omega)$ is the Greens' function was obtained.[52] P_{cav} was calculated on top of the QDs at $r_0 = 0.5 d_{QD}\, \hat{z}$ where the maximum field enhancement occurs (see Supporting Information for simulation geometry).

Supporting Information

Supporting Information is available from the Wiley Online Library or from the author.

Acknowledgements

The authors acknowledge support from European Research Council (ERC) under Horizon 2020 research and innovation programme POSEIDON (Grant Agreement No. 861950), and PICOFORCE (Grant Agreement No. 883703). NSM acknowledges support from the German National Academy of Sciences Leopoldina. L.S. acknowledges the support from the National Science Foundation under Grant No. 1905217. AD gratefully acknowledges support from the Royal Society University Research Fellowship URF\R1\180097 and URF\R\231024, Royal Society Research Fellows Enhancement Award RGF \EA\181038, and funding from EPSRC EP/X012689/1 and EP/Y008774/1. AD and AC acknowledge funding from EPSRC for the CDT in Topological Design EP/S02297X/1.

Conflict of Interest

The authors declare no conflict of interest.

Author Contributions

J.H. and J.J.B. designed the experiments. J.H. and S.H. performed sample fabrication. A.R. and L.S. synthesized the PbS QDs. A.C. and A.D. conducted finite element simulations. A.R. and Y.X. carried out TEM and AFM characterization, respectively. J.H., S.H., N.S.M, J.Y., and L.A. made the optical measurements. All authors contributed to the manuscript.

Data Availability Statement

The data that support the findings of this study are available from the corresponding author upon reasonable request.

Keywords

photoluminescence, plasmonics, purcell effect, quantum dots, stokes shift

Received: February 6, 2025
Revised: February 12, 2025
Published online: February 27, 2025

[1] S. A. McDonald, G. Konstantatos, S. Zhang, P. W. Cyr, E. J. D. Klem, L. Levina, E. H. Sargent, *Nat. Mater.* **2005**, *4*, 138.
[2] M.-J. Choi, F. P. García de Arquer, A. H. Proppe, A. Seifitokaldani, J. Choi, J. Kim, S.-W. Baek, M. Liu, B. Sun, M. Biondi, B. Scheffel, G. Walters, D.-H. Nam, J. W. Jo, O. Ouellette, O. Voznyy, S. Hoogland, S. O. Kelley, Y. S. Jung, E. H. Sargent, *Nat. Commun.* **2020**, *11*, 103.
[3] J. Tang, K. W. Kemp, S. Hoogland, K. S. Jeong, H. Liu, L. Levina, M. Furukawa, X. Wang, R. Debnath, D. Cha, K. W. Chou, A. Fischer, A. Amassian, J. B. Asbury, E. H. Sargent, *Nat. Mater.* **2011**, *10*, 765.
[4] E. V. Ushakova, A. P. Litvin, P. S. Parfenov, A. V. Fedorov, M. Artemyev, A. V. Prudnikau, I. D. Rukhlenko, A. V. Baranov, *ACS Nano* **2012**, *6*, 8913.
[5] R. Leitsmann, F. Bechstedt, *ACS Nano* **2009**, *3*, 3505.
[6] E. Jang, H. Jang, *Chem. Rev.* **2023**, *123*, 4663.
[7] F. Meinardi, A. Colombo, K. A. Velizhanin, R. Simonutti, M. Lorenzon, L. Beverina, R. Viswanatha, V. I. Klimov, S. Brovelli, *Nat. Photon* **2014**, *8*, 392.
[8] C. Li, W. Chen, D. Wu, D. Quan, Z. Zhou, J. Hao, J. Qin, Y. Li, Z. He, K. Wang, *Sci. Rep.* **2015**, *5*, 17777.
[9] S. Sadeghi, H. Bahmani Jalali, R. Melikov, B. Ganesh Kumar, M. Mohammadi Aria, C. W. Ow-Yang, S. Nizamoglu, *ACS Appl. Mater. Interfaces* **2018**, *10*, 12975.
[10] F. Meinardi, H. McDaniel, F. Carulli, A. Colombo, K. A. Velizhanin, N. S. Makarov, R. Simonutti, V. I. Klimov, S. Brovelli, *Nat. Nanotech* **2015**, *10*, 878.
[11] Y.-S. Park, J. Roh, B. T. Diroll, R. D. Schaller, V. I. Klimov, *Nat. Rev. Mater.* **2021**, *6*, 382.
[12] J. Roh, Y.-S. Park, J. Lim, V. I. Klimov, *Nat. Commun.* **2020**, *11*, 271.
[13] N. Ahn, C. Livache, V. Pinchetti, H. Jung, H. Jin, D. Hahm, Y.-S. Park, V. I. Klimov, *Nature* **2023**, *617*, 79.
[14] M. Korkusinski, O. Voznyy, P. Hawrylak, *Phys. Rev. B* **2010**, *82*, 245304.
[15] M. Nirmal, D. J. Norris, M. Kuno, M. G. Bawendi, A. L. Efros, M. Rosen, *Phys. Rev. Lett.* **1995**, *75*, 3728.
[16] D. J. Norris, A. L. Efros, M. Rosen, M. G. Bawendi, *Phys. Rev. B* **1996**, *53*, 16347.
[17] A. L. Efros, M. Rosen, M. Kuno, M. Nirmal, D. J. Norris, M. Bawendi, *Phys. Rev. B* **1996**, *54*, 4843.
[18] A. Bagga, P. K. Chattopadhyay, S. Ghosh, *Phys. Rev. B* **2006**, *74*, 035341.

[19] R. D. Schaller, S. A. Crooker, D. A. Bussian, J. M. Pietryga, J. Joo, V. I. Klimov, *Phys. Rev. Lett.* **2010**, *105*, 067403.
[20] I. Kang, F. W. Wise, *J. Opt. Soc. Am. B, JOSAB* **1997**, *14*, 1632.
[21] J. M. An, A. Franceschetti, S. V. Dudiy, A. Zunger, *Nano Lett.* **2006**, *6*, 2728.
[22] O. Voznyy, L. Levina, F. Fan, G. Walters, J. Z. Fan, A. Kiani, A. H. Ip, S. M. Thon, A. H. Proppe, M. Liu, E. H. Sargent, *Nano Lett.* **2017**, *17*, 7191.
[23] J. R. Caram, S. N. Bertram, H. Utzat, W. R. Hess, J. A. Carr, T. S. Bischof, A. P. Beyler, M. W. B. Wilson, M. G. Bawendi, *Nano Lett.* **2016**, *16*, 6070.
[24] Y. Liu, D. Kim, O. P. Morris, D. Zhitomirsky, J. C. Grossman, *ACS Nano* **2018**, *12*, 2838.
[25] M. Pelton, *Nat. Photon* **2015**, *9*, 427.
[26] G. M. Akselrod, M. C. Weidman, Y. Li, C. Argyropoulos, W. A. Tisdale, M. H. Mikkelsen, *ACS Photonics* **2016**, *3*, 1741.
[27] G. M. Akselrod, C. Argyropoulos, T. B. Hoang, C. Ciracì, C. Fang, J. Huang, D. R. Smith, M. H. Mikkelsen, *Nat. Photon* **2014**, *8*, 835.
[28] T. B. Hoang, G. M. Akselrod, C. Argyropoulos, J. Huang, D. R. Smith, M. H. Mikkelsen, *Nat. Commun.* **2015**, *6*, 7788.
[29] A. Rose, T. B. Hoang, F. McGuire, J. J. Mock, C. Ciracì, D. R. Smith, M. H. Mikkelsen, *Nano Lett.* **2014**, *14*, 4797.
[30] J. Huang, S. Hu, D. Kos, Y. Xiong, L. A. Jakob, A. Sánchez-Iglesias, C. Guo, L. M. Liz-Marzán, J. J. Baumberg, *ACS Nano* **2024**, *18*, 3323.
[31] J. J. Baumberg, J. Aizpurua, M. H. Mikkelsen, D. R. Smith, *Nat. Mater.* **2019**, *18*, 668.
[32] J. Huang, D.-B. Grys, J. Griffiths, B. de Nijs, M. Kamp, Q. Lin, J. J. Baumberg, *Sci. Adv.* **2021**, *7*, eabg1790.
[33] H. Groß, J. M. Hamm, T. Tufarelli, O. Hess, B. Hecht, *Sci. Adv.* **2018**, *4*, aar4906.
[34] H. Leng, B. Szychowski, M.-C. Daniel, M. Pelton, *Nat. Commun.* **2018**, *9*, 4012.
[35] J. Huang, O. S. Ojambati, R. Chikkaraddy, K. Sokołowski, Q. Wan, C. Durkan, O. A. Scherman, J. J. Baumberg, *Phys. Rev. Lett.* **2021**, *126*, 047402.
[36] Z. C. Dong, X. L. Zhang, H. Y. Gao, Y. Luo, C. Zhang, L. G. Chen, R. Zhang, X. Tao, Y. Zhang, J. L. Yang, J. G. Hou, *Nat. Photon* **2010**, *4*, 50.
[37] A. M. Flatae, F. Tantussi, G. C. Messina, F. De Angelis, M. Agio, *J. Phys. Chem. Lett.* **2019**, *10*, 2874.
[38] N. S. Mueller, R. Arul, G. Kang, A. P. Saunders, A. C. Johnson, A. Sánchez-Iglesias, S. Hu, L. A. Jakob, J. Bar-David, B. de Nijs, L. M. Liz-Marzán, F. Liu, J. J. Baumberg, *Nat. Commun.* **2023**, *14*, 5726.
[39] N. Reilly, M. Wehrung, R. A. O'Dell, L. Sun, *Mater. Chem. Phys.* **2014**, *147*, 1.
[40] R. T. Hill, J. J. Mock, A. Hucknall, S. D. Wolter, N. M. Jokerst, D. R. Smith, A. Chilkoti, *ACS Nano* **2012**, *6*, 9237.
[41] E. Elliott, K. Bedingfield, J. Huang, S. Hu, B. de Nijs, A. Demetriadou, J. J. Baumberg, *ACS Photonics* **2022**, *9*, 2643.
[42] C. Cheng, J. Li, X. Cheng, *J. Lumin.* **2017**, *188*, 252.
[43] M. S. Gaponenko, A. A. Lutich, N. A. Tolstik, A. A. Onushchenko, A. M. Malyarevich, E. P. Petrov, K. V. Yumashev, *Phys. Rev. B* **2010**, *82*, 125320.
[44] J. H. Warner, E. Thomsen, A. R. Watt, N. R. Heckenberg, H. Rubinsztein-Dunlop, *Nanotechnology* **2004**, *16*, 175.
[45] L. A. Jakob, W. M. Deacon, O. Hicks, I. Manyakin, O. S. Ojambati, M. Traxler, J. J. Baumberg, *Optica* **2021**, *8*, 1646.
[46] V. I. Klimov, D. W. McBranch, C. A. Leatherdale, M. G. Bawendi, *Phys. Rev. B* **1999**, *60*, 13740.
[47] A. A. Bakulin, S. Neutzner, H. J. Bakker, L. Ottaviani, D. Barakel, Z. Chen, *ACS Nano* **2013**, *7*, 8771.
[48] A. R. Salmon, M.-E. Kleemann, J. Huang, W. M. Deacon, C. Carnegie, M. Kamp, B. de Nijs, A. Demetriadou, J. J. Baumberg, *ACS Nano* **2020**, *14*, 4982.
[49] N. Kongsuwan, A. Demetriadou, M. Horton, R. Chikkaraddy, J. J. Baumberg, O. Hess, *ACS Photonics* **2020**, *7*, 463.
[50] J. Huang, O. S. Ojambati, C. Climent, A. Cuartero-Gonzalez, E. Elliott, J. Feist, A. I. Fernández-Domínguez, J. J. Baumberg, *ACS Nano* **2024**, *18*, 14487.
[51] A. Dong, J. Chen, P. M. Vora, J. M. Kikkawa, C. B. Murray, *Nature* **2010**, *466*, 474.
[52] L. Novotny, B. Hecht, in *Principles of Nano-Optics*, Cambridge University Press, Cambridge **2006**.